Results in Physics 7 (2017) 413–425

Contents lists available at ScienceDirect

Results in Physics

journal homepage: www.journals.elsevier.com/results-in-physics

# Dynamics of variable-viscosity nanofluid flow with heat transfer in a flexible vertical tube under propagating waves

A. Bintul Huda [a,*], Noreen Sher Akbar [b], O. Anwar Beg [c], M. Yaqub Khan [a]

[a] Mathematics & Statistics Department Riphah International University I-14, Islamabad, Pakistan
[b] DBS&H, CEME, National University of Sciences and Technology, Islamabad, Pakistan
[c] Fluid Mechanics, Spray Research Group, School of Computing, Science and Engineering, Newton Bldg, G77, University of Salford, Manchester M54WT, UK

ARTICLE INFO

*Article history:*
Received 10 November 2016
Accepted 24 December 2016
Available online 5 January 2017

*Keywords:*
Biophysics
Heat transfer
Flexible tube
Temperature-dependent viscosity
Nanoparticles
Drug delivery

ABSTRACT

*Background and objectives:* The present investigation addresses nanofluid flow and heat transfer in a vertical tube with temperature-dependent viscosity. A Tiwari-Das type formulation is employed for the nanofluid with a viscosity modification. As geometry of the problem is flexible tube so flow equations are modeled considering cylindrical coordinates. Governing partial differential equations are simplified and converted into differential equations using non-dimensionless variables with low Reynolds number ($\mathrm{Re} \ll 0$ i.e. inertial forces are small as compared to the viscous forces) and long wavelength ($\delta \ll 0$ i.e. physiologically valid that length of tube is very large as compared to width of the tube) approximations. *Methods results conclusions:* Mathematica software is employed to evaluate the exact solutions of velocity profile, temperature profile, axial velocity profile, pressure gradient and stream function. The influence of heat source/sink parameter ($\beta$), Grashof number ($G_r$) and the viscosity parameter ($\alpha$) and nanoparticle volume fraction ($\phi$) on velocity, temperature, pressure gradient, pressure rise and wall shear stress distributions is presented graphically. Three different nanofluid suspensions are investigated- Titanium oxide-water, Copper oxide-water and Silver-water. Streamline plots are also computed to illustrate bolus dynamics and trapping phenomena which characterize peristaltic propulsion. The computations show that wall shear stress is maximum for the Silver-water nanofluid case. Furthermore the pressure rise is reduced with increasing Grashof number, heat absorption parameter and viscosity parameter in the augmented pumping region whereas the contrary response is observed in the peristaltic pumping region. Significant modification in the quantity of trapped boluses is found with different nanofluids and the size of the trapped bolus decreased in the Titanium oxide-water nanofluid case with either greater heat source or sink parameter. The study is relevant to drug delivery systems exploiting nano-particles.



## Introduction

Peristaltic transport is a biological mechanism which entails the conveyance of material induced by a progressive wave of contraction or expansion along the length of a distensible vessel (tube). This effectively mixes and propels the fluid in the direction of the wave propagation. Peristaltic flows of non-Newtonian viscous fluids are encountered in many complex physiological systems including urine transport from the kidney to the bladder, chyme motion in the gastrointestinal tract, movement of ovum in the female fallopian tube, vasomotion of small blood vessels, transport of spermatozoa, and swallowing food through the esophagus (and other biomedical applications which are summarized in Fung [1]) and also phloem *trans*-location in plants as described by Thaine [2] and Thompson [3]. In a mathematical context, peristaltic flows fall in the category of *moving boundary value problems*. They have as a result mobilized considerable interest in recent years. Many analytical investigations of peristaltic propulsion have therefore been communicated and these have addressed a diverse range of geometries under various assumptions such as large wavelength, small amplitude ratio, small wave number, small Deborah number, low Reynolds number and creeping flow, etc. Representative works in this regard include Ellahi [4]; Hameed and Nadeem, [5]; Tan and Masuoka, [6–8]; Mahomed and Hayat, [9]; Fetecau and Fetecau, [10]; Malik et al., [11]; Dehghan and Shakeri, [12]. Some relevant studies on the topic can be found from the list of references (Nadeem and Akbar, [13,14]) and several references therein. Simulations of peristalsis, which is derived from the Greek word *peristalitikos*, which means clasping and compressing, are also of

* Corresponding author.
*E-mail address:* abhripha@gmail.com (A.B. Huda).

http://dx.doi.org/10.1016/j.rinp.2016.12.036
2211-3797/

great relevance to advanced medical and biochemical engineering pumps. Roller and Finger pumps using viscous fluid operate on this principle. Peristaltic pumps offer considerable advantages over conventional pumping mechanisms including corrosion mitigation and leak-free designs. Furthermore such pumps can avoid internal backflow and thereby can consistently deliver accurate dosing without slip and exhibit excellent repeatability and metering capabilities. The tube components in peristaltic pumps also achieve longer service times and minimize maintenance. They have therefore been deployed in many diverse areas of biomedicine including diabetic treatment [15] and drug delivery in cancer therapy [16]. They have also been integrated into medical recirculating cooling pumps with applications in cooling electro-tips of RF catheters in order to mitigate blood coagulation on the tip during ablation therapy. The mechanism of peristaltic transport has also been exploited in biohazard management including sanitary fluid transport and safe conveyance of corrosive fluid where the contact of the fluid with the machinery parts is prohibited. Further details are provided in Diniz et al. [17].

Non-Newtonian models are extremely diverse and include viscoelastic, viscoplastic, micro-continuum and other formulations. Variable-viscosity models are also an important sub-section of rheological liquids. They have therefore also been investigated in the context of peristaltic flows, since viscosity variation (e.g. with temperature) is an important characteristic of certain physiological (and industrial) materials. Peristaltic transport of a power-law fluid with variable consistency was examined by Shukla and Gupta [18]. They observed that for zero pressure drop, flow rate flux is elevated for greater amplitude of the peristaltic wave whereas it is suppressed with increasing pseudo-plastic nature of the fluid. They further noted that wall friction is reduced as the consistency decreases. Srivastava et al. [19] studied the peristaltic transport of a fluid with variable viscosity through a non-uniform tube. They showed that the pressure rise is markedly lowered as the fluid viscosity decreases at zero flow rate but is infact independent of viscosity variation at a certain value of flow rate. However beyond this critical flow rate, the pressure rise is enhanced with greater viscosity. Abd El Hakeem et al. [20] studied using perturbation expansions, the influence of variable viscosity and an inserted endoscope on peristaltic viscous flow. They employed an exponential decay model for viscosity and observed that pressure rise is decreased with increasing viscosity ratio whereas it is enhanced with increasing wave number, amplitude ratio and radius ratio. Further studies of variable-viscosity peristaltic flow include Abd El Hakeem et al. [21] for magnetohydrodynamic fluids, Khan et al. [22] for inclined pumping of non-Newtonian fluids and Akbar [23] present nanoparticle volume fraction for phase model.

Another significant development in medical engineering in recent years has been the emergence of *nanofluids*, a subcategory of nanoscale materials. Nanofluids comprise base fluids (water, air, ethylene glycol etc) with nano-size solid particles suspended in them. Nanofluids have gained much attention from investigators due to their high thermal conductivity and pioneering work in developing such fluids was first performed by Choi [24] Nanoparticles are generally synthesized from metals, oxides, carbides, or carbon nanotubes owing to high thermal conductivities associated with these materials. In a medical engineering context as refer in [24], nanoparticles have been found to achieve exceptional performance in enhancing thermal and mass diffusion properties of, for example, drugs injected into the blood stream. Biocompatability of the selected metallic oxides is crucial for safe deployment of nanofluids in medicine. New potential applications for nanoparticles in nanoparticle blood diagnostic systems, asthma sensors, carbon nanotubes in catheters and stents and anti-bacterial treatment for wounds via peristaltic pump delivery was identified by Harris and Graffagnini [25]. Nanoparticles possess many unique attributes which make them particularly attractive for clinical applications. These include a surface to mass ratio which is much greater than that of other particles, site-specific targeting features which can be achieved by attaching targeting ligands to surface of particles (or via magnetic guidance), quantum properties, enhanced ability to adsorb and carry other compounds, excellent large functional surface which can bind, adsorb and convey secondary compounds (drugs, probes and proteins). Further advantages encompass controllable deployment of particle degradation characteristics which can be successfully modulated by judicious selection of matrix constituents, and flexibility in administration methods (nasal, parenteral, intra-ocular). In neuro-pharmacological hemodynamics as refer in [26], it has been clinically verified that nanoparticles can easily penetrate the blood brain barrier (BBB) facilitating the introduction of therapeutic agents into the brain. Fullstone et al. [26] have also recently described the exceptional characteristics of nanoparticles (size, shape and surface chemistry) in assisting effective delivery of drugs within cells or tissue (achieved via modulation of immune system interactions, blood clearance profile and interaction with target cells). They have further shown that erythrocytes aid in effective nanoparticle distribution within capillaries. Further studies include Tan et al. [27]. Simulation of peristaltic flows of nanoparticles is therefore extremely relevant to improve administration of nanofluids in medicine. Representative studies in this regard include Tripathi and Bég [28] who considered analytically the thermal and nano-species buoyancy effects on heat, mass and momentum transfer in peristaltic propulsion of nanofluids in peristaltic pumping devices, employing the Buongiornio formulation which incorporates Brownian motion and thermophoresis. Ebaid and Aly [29] studied magnetic field effects on electrically-conducting nanofluid propulsion by peristaltic waves with applications in cancer therapy. Akbar et al. [30] investigated peristaltic slip nanofluid hydrodynamics in an asymmetric channel, obtaining series solutions for temperature, nano-particle concentration, stream function and pressure gradient. Akbar and Nadeem [31] considered peristaltic flow of Phan-Thien-Tanner nanofluid in a diverging conduit with the homotopy perturbation method. Further analyses include Bég and Tripathi [32] who considered double-diffusive convection of nanofluids in finite length pumping systems. These studies did not consider variable viscosity effects. Further literature can be viewed through Refs. [33–44].

In the present article, we therefore consider the peristaltic propulsion of nanofluid in a vertical conduit with temperature-dependent viscosity. Basic formulation is employed for the nanofluid with a viscosity modification. Heat transfer is also considered and heat source/sink and thermal buoyancy effects featured. Various nano-particles are considered i.e. Titanium oxide-water, Copper oxide-water and Silver-water. Analytical solutions are derived to examine the effects of heat generation/absorption parameter, Grashof number, viscosity parameter and nanoparticle volume fraction on velocity, temperature, pressure gradient, pressure rise and wall shear stress variables. Streamline visualization is also computed to assess trapping hydrodynamics. The mathematical model is of potential importance in better understanding medical peristaltic pump nano-pharmacological delivery systems.

## Nanofluid peristaltic transport model

Consider axisymmetric flow of a variable-viscosity nanofluid in a circular tube of finite length, $L$. The tube walls are flexible and a sinusoidal wave propagates along the walls of the tube. Isothermal conditions are enforced at the walls which are maintained at a temperature, $T_0$. At the center of the tube, a symmetric

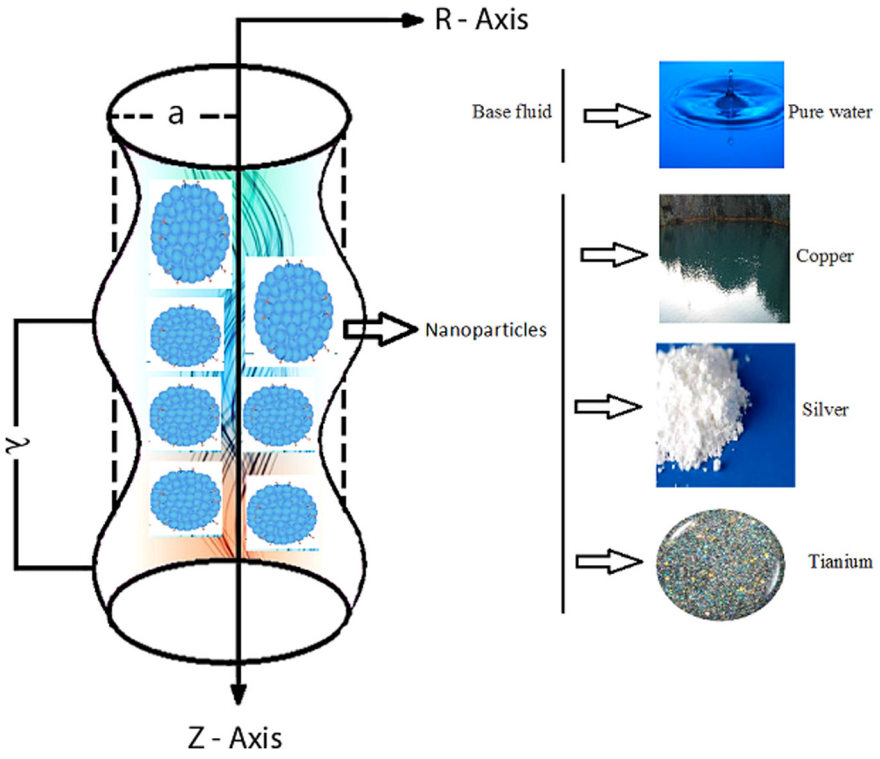


**Fig. 1.** Geometry of problem.

temperature condition is imposed. The geometric model is illustrated in Fig. 1 with respect to a cylindrical coordinate system $(\bar{R}, \bar{Z})$.

The geometry of the wall surface is simulated via the following relation:

$$\bar{h} = a + b\sin\frac{2\pi}{\lambda}(\bar{Z} - c\bar{t}), \tag{1}$$

where $\bar{h}$ denotes the height of the tube wall, $a$ denotes the radius of the tube, $b$ is the wave amplitude, $\lambda$ is the wave length and $c$ is the peristaltic wave speed. In the fixed coordinates system $(\bar{R}, \bar{Z})$, the hydrodynamics is *unsteady*. It becomes *steady* in a wave frame $(\bar{r}, \bar{z})$ moving with the same speed as the wave moves in the $\bar{Z}$-direction. The transformations between the two frames (i.e. laboratory and wave frame) are:

$$\bar{r} = \bar{R}, \bar{z} = \bar{Z} - c\bar{t}, \ \bar{v} = \bar{V}, \ \bar{w} = \bar{W} - c, \ \bar{p}(\bar{z}, \bar{r}, \bar{t}) = \bar{p}(\bar{Z}, \bar{R}, \bar{t}), \tag{2}$$

The governing equations for conservation of mass, momentum and heat (energy) of an incompressible nanofluid, assuming the nanofluid to be a dilute suspension in thermal equilibrium, may be written as:

$$\frac{1}{\bar{r}}\frac{\partial(\bar{r}\bar{u})}{\partial\bar{r}} + \frac{\partial\bar{w}}{\partial\bar{z}} = 0, \tag{3}$$

$$\rho_{nf}\left[\bar{u}\frac{\partial\bar{u}}{\partial\bar{r}} + \bar{w}\frac{\partial\bar{u}}{\partial\bar{r}}\right] = -\frac{\partial\bar{p}}{\partial\bar{r}} + \frac{\partial}{\partial\bar{r}}\left[2\mu_{nf}(\theta)\frac{\partial\bar{u}}{\partial\bar{r}}\right] + \mu_{nf}(\theta)\frac{2}{\bar{r}}\left(\frac{\partial\bar{u}}{\partial\bar{r}} - \frac{\bar{u}}{\bar{r}}\right) + \frac{\partial}{\partial\bar{z}}\left[\mu_{nf}(\theta)\left(\frac{\partial\bar{u}}{\partial\bar{r}} + \frac{\partial\bar{w}}{\partial\bar{z}}\right)\right], \tag{4}$$

$$\rho_{nf}\left[\bar{u}\frac{\partial\bar{w}}{\partial\bar{r}} + \bar{w}\frac{\partial\bar{w}}{\partial\bar{z}}\right] = -\frac{\partial\bar{p}}{\partial\bar{z}} + \frac{1}{\bar{r}}\frac{\partial}{\partial\bar{r}}\left[\mu_{nf}(\theta)\bar{r}\left(\frac{\partial\bar{u}}{\partial\bar{z}} + \frac{\partial\bar{w}}{\partial\bar{r}}\right)\right] + \frac{\partial}{\partial\bar{z}}\left[2\mu_{nf}(\theta)\frac{\partial\bar{w}}{\partial\bar{z}}\right] + (\rho\gamma)_{nf}g(\bar{T} - T_0), \tag{5}$$

$$\frac{\partial\bar{T}}{\partial\bar{t}} + \bar{u}\frac{\partial\bar{T}}{\partial\bar{r}} + \bar{w}\frac{\partial\bar{T}}{\partial\bar{z}} = \frac{k_{nf}}{(\rho_{cp})_{nf}}\left[\frac{\partial^2\bar{T}}{\partial\bar{r}^2} + \frac{1}{\bar{r}}\frac{\partial\bar{T}}{\partial\bar{r}} + \frac{\partial^2\bar{T}}{\partial\bar{z}^2}\right] + \frac{Q_0}{(\rho_{cp})_{nf}}. \tag{6}$$

where $\bar{r}$ and $\bar{z}$ are the co-ordinates in the wave frame. $\bar{z}$ is taken as the center line of the tube and $\bar{r}$ is orientated transverse to it, $\bar{u}$ and $\bar{w}$ are the velocity components in the $\bar{r}$ and $\bar{z}$ directions respectively, $\bar{T}$ is the local temperature of the fluid. Further $\mu_{nf}$ is the effective dynamic viscosity of nanofluid, $\alpha_{nf}$ is the effective thermal diffusivity of nanofluid, $\rho_{nf}$ is the effective density of nanofluid, $(\rho c_p)_{nf}$ is the heat capacitance of the nanofluid and $k_{nf}$ is the effective thermal conductivity of the nanofluid, and the subscript *s designates solid*. These are defined, respectively, as follows:

$$\begin{aligned}
&\mu_{nf} = \frac{\mu_0 e^{-\alpha\theta}}{(1-\phi)^{2.5}}, \ \alpha_{nf} = \frac{k_{nf}}{(\rho c_p)_{nf}}, \ \rho_{nf} = (1-\phi)\rho_f + \phi\rho_s,\\
&(\rho c_p)_{nf} = (1-\phi)(\rho c_p)_f + \phi(\rho c_p)s, \ (\rho\gamma)_{nf} = (1-\phi)(\rho\gamma)_f + \phi(\rho\gamma)_S,\\
&k_{nf} = k_f\left(\frac{k_s + 2k_f - 2\phi(k_f - k_s)}{k_s + 2k_f + 2\phi(k_f - k_s)}\right)
\end{aligned} \tag{7}$$

In above equation $\rho_f$ density of the base fluid, $\rho_s$ density of the nanoparticles, $k_f$ thermal conductivity of the base fluid, $k_s$ thermal conductivity of the nanoparticles, $\gamma_{nf}$ is the thermal expansion coefficient, $\gamma_f$ is the thermal expansion coefficient of basefluid $\phi$ is the nanoparticle volume fraction, and $\gamma_s$ is the thermal expansion coefficient of the nanoparticles.

We introduce the following non-dimensional variables:

$$\begin{aligned}
&r = \frac{\bar{r}}{a}, \ z = \frac{\bar{z}}{\lambda}, \ w = \frac{\bar{w}}{c}, \ u = \frac{\lambda\bar{u}}{ac}, \ p = \frac{a^2\bar{p}}{c\lambda\mu_f}, \ \theta = \frac{(\bar{T} - \bar{T}_0)}{\bar{T}_0}, \ t = \frac{c\bar{t}}{\lambda},\\
&\varepsilon = \frac{b}{a}, \ G_r = \frac{g\alpha a^2 T_0\rho_{nf}}{c\mu_f}, \ \beta = \frac{Q_0 a^2}{k_f T_0}.
\end{aligned} \tag{8}$$

These represent respectively the r dimensionless radial coordinate, z dimensionless axial coordinate, w,u dimensionless radial and axial velocity components, p dimensionless pressure, $\theta$ dimensionless temperature function, t dimensionless time, $\varepsilon$ radius ratio,

$G_r$ Grashof number and β heat source/sink parameter. Implementing these variables in Eqs. (2)–(5) and invoking the assumptions of low Reynolds number and long wavelength, the non-dimensional governing equations after dropping the dashes can be written as the following steady-state equations in the wave frame.

$$\frac{\partial p}{\partial r} = 0, \tag{9}$$

$$\frac{dp}{dz} = \frac{1}{r}\frac{\partial}{\partial r}\left(\frac{\mu_{nf}}{\mu_0}\left(r\frac{\partial w}{\partial r}\right)\right) + \frac{(\rho\gamma)_{nf}}{(\rho\gamma)_f}G_r\theta, \tag{10}$$

$$\frac{\partial^2\theta}{\partial r^2} + \frac{1}{r}\frac{\partial\theta}{\partial r} + \beta\frac{k_f}{k_{nf}} = 0, \tag{11}$$

The Reynolds model for nanofluid viscosity can be defined as follows:

$$\frac{\mu_{nf}}{\mu_0} = \frac{e^{-\alpha\theta}}{(1-\phi)^{2.5}}, \quad \text{and} \quad e^{-\alpha\theta} = 1-\alpha\theta, \quad \alpha \ll 1. \tag{12}$$

where α is the viscosity parameter and $\mu_0$ constant viscosity of the fluid.

The non-dimensional boundary conditions are prescribed as:

$$\frac{\partial w}{\partial r} = 0, \frac{\partial\theta}{\partial r} = 0 \quad \text{at} \quad r = 0, \tag{13}$$

$$w = -1, \ \theta = 0, \quad \text{at} \quad r = h(z) \quad \text{where} \quad h(z) = 1 + \varepsilon\cos(2\pi z) \tag{14}$$

## Analytical solutions of the boundary value problem

Closed-form solutions are feasible for the transformed, non-dimensional boundary value problem. Solving Eqs. (9)–(11) together with boundary conditions (13) and (14) therefore generates the following expressions for *temperature* and *axial velocity*:

$$\theta(r,z) = \frac{1}{4}\left(\left(\frac{k_s + 2k_f + 2\phi(k_f - k_s)}{k_s + 2k_f - 2\phi(k_f - k_s)}\right)\right)\beta(h^2 - r^2). \tag{15}$$

$$w(r,z) = \frac{dP}{dz}(1-\phi)^{2.5}\left(L_3\frac{(r^2-h^2)}{4} - L_4\frac{(r^4-h^4)}{8}\right) + \left((1-\phi) + \phi\frac{(\rho\gamma)_s}{(\rho\gamma)_f}\right)$$
$$G_r(1-\phi)^{2.5}\left(L_5\frac{(r^2-h^2)}{2} + L_6\frac{(r^4-h^4)}{4} + L_7\frac{(r^6-h^6)}{6}\right). \tag{16}$$

where:

$$K = \frac{k_f}{k_{nf}}, \ L = ((1-\phi)(\rho_f\gamma_f) + \phi(\rho_s\gamma s))/(\rho_f\gamma_f) L_1 = L\frac{G_r\beta K}{4}, \ L_2 = \frac{(1-\phi)^{2.5}}{2},$$
$$L_3 = \frac{L_1 h^2}{2}(1-\phi)^{2.5}, \ L_4 = -\frac{L_1}{4}(1-\phi)^{2.5}, \ L_5 = L_2 + L_2\frac{\alpha\beta K h^2}{4}, \ L_6 = -L_2\frac{\alpha\beta K}{4},$$
$$L_7 = -L_3 - L_3\frac{\alpha\beta K h^2}{4}, \ L_8 = -L_4 + L_3\frac{\alpha\beta K}{4} - L_4\frac{\alpha\beta K h^2}{4}, \ L_9 = L_4\frac{\alpha\beta K}{4} \tag{17}$$

The *volumetric flow rate* of nanofluid in the tube is given by:

$$F = \int_0^{h(z)} rw dr, \tag{18}$$

Axial pressure gradient emerges as:

$$\frac{dp}{dz} = \frac{F - h^4 L_9(1-\phi)^{2.5}\left((1-\phi) + \phi\frac{(\rho\gamma)_s}{(\rho\gamma)_f}\right)}{h^4 L_8(1-\phi)^{2.5}} \tag{19}$$

It follows that the *mean flow rate* is given by:

$$F = 2Q - \frac{\varepsilon^2}{2} - 1, \tag{20}$$

Integrating Eq. (19) over the interval [0,1] leads to an expression for the *pressure rise*:

$$\Delta P = \int_0^1 \left(\frac{dp}{dz}\right) dz. \tag{21}$$

Expression of wall shear stress is evaluated using

$$S_{rz} = \left.\frac{\partial w}{\partial r}\right|_{r=h}, \tag{22}$$

## Results and discussion

Numerical computations, based on the exact solutions derived in Section "Analytical solutions of the boundary value problem", have been conducted to assess the influence of flow parameters

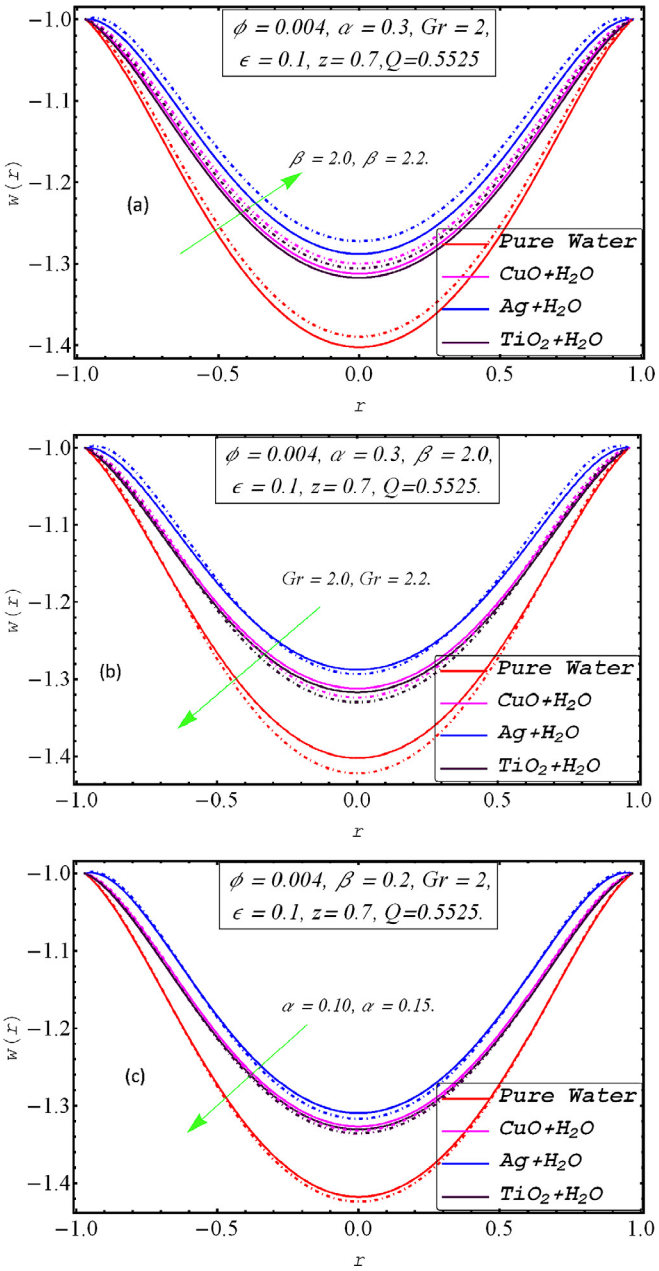


**Fig. 2.** Velocity profile for different values of the (a) $\beta = 2.0, 2.2$. (b) $Gr = 2.0, 2.2$ and (c) $\alpha = 0.10, 0.15$. (Red line Pure water — Purple line Cuo + $H_2O$ — Blue line Ag + $H_2O$ — Dark Purple line TiO2 + $H_2O$ —). (For interpretation of the references to color in this figure legend, the reader is referred to the web version of this article.)

on the peristaltic flow characteristics. These are depicted in Figs. 2–12. These computations are based on nanofluid properties documented in Table 1. Further solutions are given for the velocity and temperature fields in Tables 2–4.

Fig. 2($a$)–($c$) depict the velocity evolution in the tube for different values of $\beta$, $G_r$ and $\alpha$. It is observed that when we increase the value of heat absorption parameter $\beta$, the velocity of the pure water and other nanoparticles also increases (Fig. 2a). Heat introduction into the fluid therefore enhances momentum transfer also and accelerates the axial flow. Parabolic distributions are observed across the tube diameter, with the core flow accelerated substantially due to greater heat source (absorption). Note the solid colored lines correspond to $\beta = 2.0$ whereas the dotted color lines are associated with $\beta = 2.2$. Axial velocity is maximized with silver-water ($Ag + H_2o$) nanofluid, whereas it is minimized with pure water. Copper-water nanofluid also achieves slightly greater acceleration in the core flow than does Tianium oxide nanofluid, however both under-perform compared with silver-nanofluid. It is also apparent in Fig. 2b, that with an increment in Grashof number, $G_r$, nanofluid velocity is significantly decreased i.e. flow deceleration is induced across the tube diameter. Once again the silver-water nanofluid achieves the best acceleration, and out-performs the Copper water nanofluid, titaniums oxide nanofluid and achieves dramatically greater velocities than pure water. The Grashof number is a representation of thermal buoyancy effect relative to viscous hydrodynamic force. When $Gr = 1$ these forces are the same order of magnitude in the tube. For $Gr > 1$ thermal buoyancy force exceeds viscous force and vice versa for $Gr < 1$. Thermal buoyancy is known to decelerate viscous flows, since it opposes momentum development and inhibits propulsion in the tube. This observation is consistent with many other studies on peristaltic nanofluids, including [33–40]. Fig. 2c shows that an increase in viscosity parameter ($\alpha$), decreases the axial velocity, again especially in the core region. Because increasing in viscosity parameter there will be more resistance in the fluid that will reduce the velocity. As solid lines are for small viscosity parameters dotted lines are for large values of viscosity parameter so raising the viscosity parameter there is decline in the velocity. Based on the Reynolds model (Reynolds 1886), originally for non-Newtonian tribological flows, the nanofluid viscosity will decrease with increasing values of $\alpha$; and higher temperature ($\theta$). This will reduce the viscous forces in the fluid and will lead to acceleration, as observed in Fig. 2c. pure water is found to sustain significant deceleration as compare with the nanofluid cases. Again Silver water nanofluid achieves the best acceleration in the core flow.

Fig. 3($a$)–($b$) present the radial temperature distributions, $\theta(r)$ with variation in heat source parameter ($\beta$) and nano-particle volume fraction ($\phi$). Significant elevation in temperature is sustained as the increases in heat absorption parameter. Maximum temperatures are attained for pure water and the minimum temperatures are associated with silver-water nanofluid. Copper water nanofluid achieves greater temperatures than silver water nanofluid but

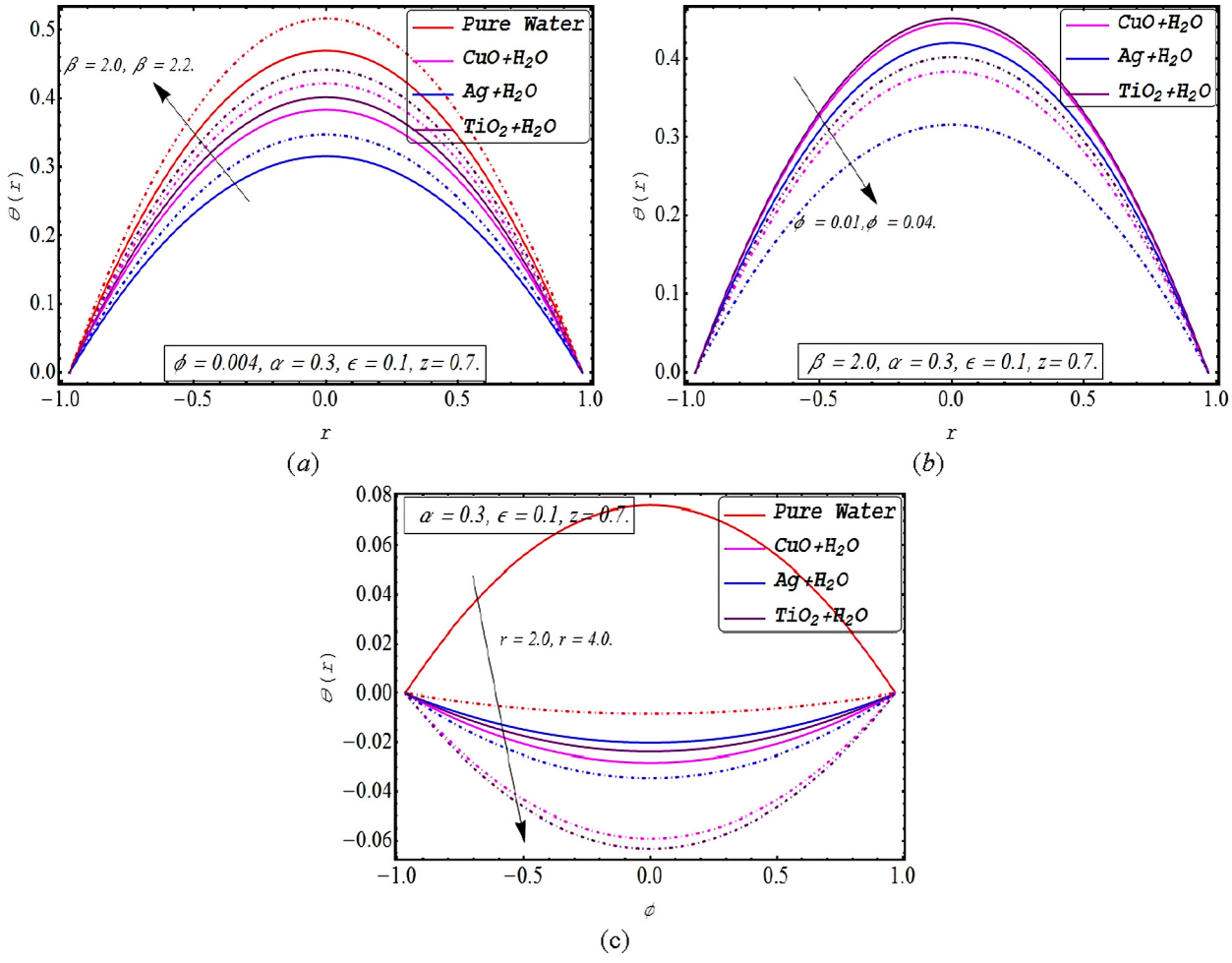


**Fig. 3.** Temperature profile against the radial axis $r$ for different values of (a) $\beta = 2.0, 2.2$. (b) $\phi = 0.01, 0.04$ and (c) r = 2.0, 4.0. (Red line Pure water ——— Purple line Cuo + $H_2O$ ——— Blue line Ag + $H_2O$ ——— Dark Purple line TiO2 + $H_2O$ ———). (For interpretation of the references to color in this figure legend, the reader is referred to the web version of this article.)

distinctly lower temperatures than Titanium oxide nanofluid. Silver water nanofluid therefore generally demonstrates the *best cooling performance* compared with pure water and nanofluids as it successfully minimizes temperature increase in the flow. This pattern of behavior is also confirmed by increasing the nanoparticle volume fraction $\varphi$ (Fig. 3b) where again silver water nanofluid is found to consistently attain the lowest temperatures. With increasing nano-particle volume fraction, the desired effect of cooling the pumping fluid is achieved. Titanium water nanofluid is observed to produce the highest temperatures, then Copper water nanofluid and finally silver water nanofluid. Therefore for temperature regulation in peristaltic nanofluid pumping, the optimized cooling performance is associated with Silver water nanofluids. In all cases symmetric parabolic distributions are observed across the tube cross-section, and the maximum temperature always arises at the tube centerline.

Fig. 4(a)–(c) present the evolution of axial pressure gradient along the tube (i.e. with axial coordinate). The magnitudes of pressure gradient decrease with greater heat absorption parameter ($\beta$) as shown in Fig. 3a. Values are highest for Titanium oxide and lowest for Silver water nanofluid. Values are also generally maximized at the central zone of the tube length but are clearly non-zero both at the entry of the tube (z = 0) and at the exit ($z$ = 1.0). A pressure gradient is therefore maintained throughout the tube irrespective of whether pure water or nanofluid is the transported material. Copper water nanofluid achieves greater pressure gradient magnitudes than silver water nanofluid but substantially lower values than Titanium oxide nanofluid. Fig. 4b shows that with increasing Grashof number, $G_r$, a similar response in pressure gradient is computed i.e. it decreases significantly throughout the length of the tube. Increasing thermal buoyancy force in the peristaltic flow regime therefore depresses pressure gradient consistently. Maximum magnitudes are again noted for Titanium oxide nanofluid whereas the lowest magnitudes correspond to Silver water nanofluid. This has implications in clinical applications, since for sustaining greater pressure gradients, which affect the efficiency of delivery of drugs, Titanium oxide nano-particles would potentially perform better than the other nano-particles. Fig. 4c illustrates that with *increasing viscosity parameter* ($\alpha$) which is associated with *decreasing nanofluid dynamic viscosity* ($\mu_{nf}$, based on Reynolds exponential decay model, Eq. (12)), pressure gradient is substantially elevated. Titanium oxide nanofluid is observed to achieve the peak values of pressure gradient and Silver water nanofluid again produces the lowest magnitudes. Overall therefore irrespective of the parameter being varied, Titanium oxide nanofluid prevails as the best choice for sustaining high axial pressure gradient values in peristaltic nanofluid propulsion.

Fig. 5(a)–(c) provide an insight into the response in pressure rise ($\Delta p$) with a variation in heat absorption, Grashof number and viscosity parameter, respectively. Again pure water and three

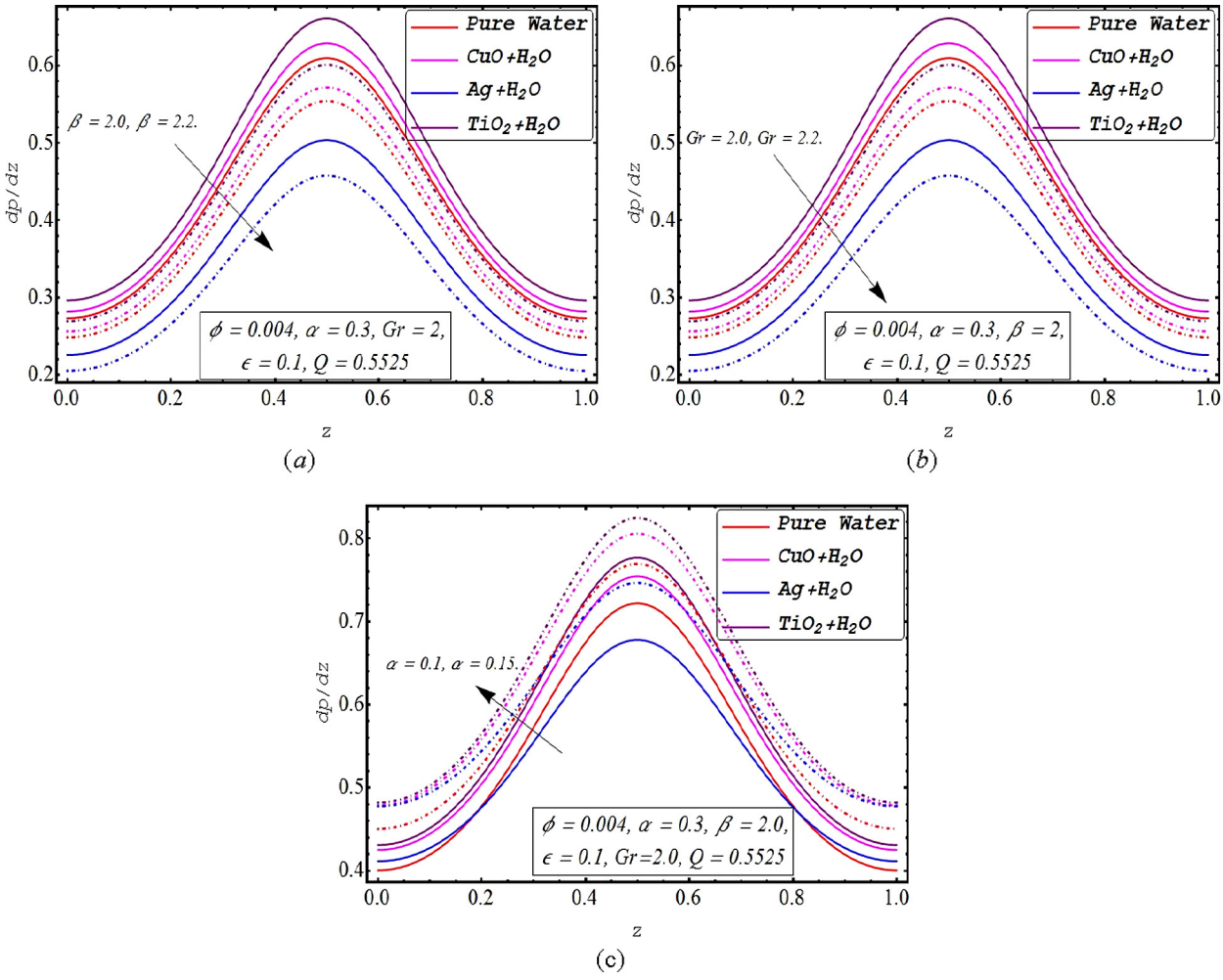


**Fig. 4.** Pressure gradient $\frac{dp}{dz}$ against the axial distance $z$ for different values of (a) $\beta$ = 2.0 , 2.2. (b) $Gr$ = 2.0, 2.2 and (c) $\alpha$ = 0.10, 0.15. (Red line Pure water ——— Purple line Cuo + $H_2O$ ——— Blue line Ag + $H_2O$ ——— Dark Purple line TiO2 + $H_2O$ ———). (For interpretation of the references to color in this figure legend, the reader is referred to the web version of this article.)

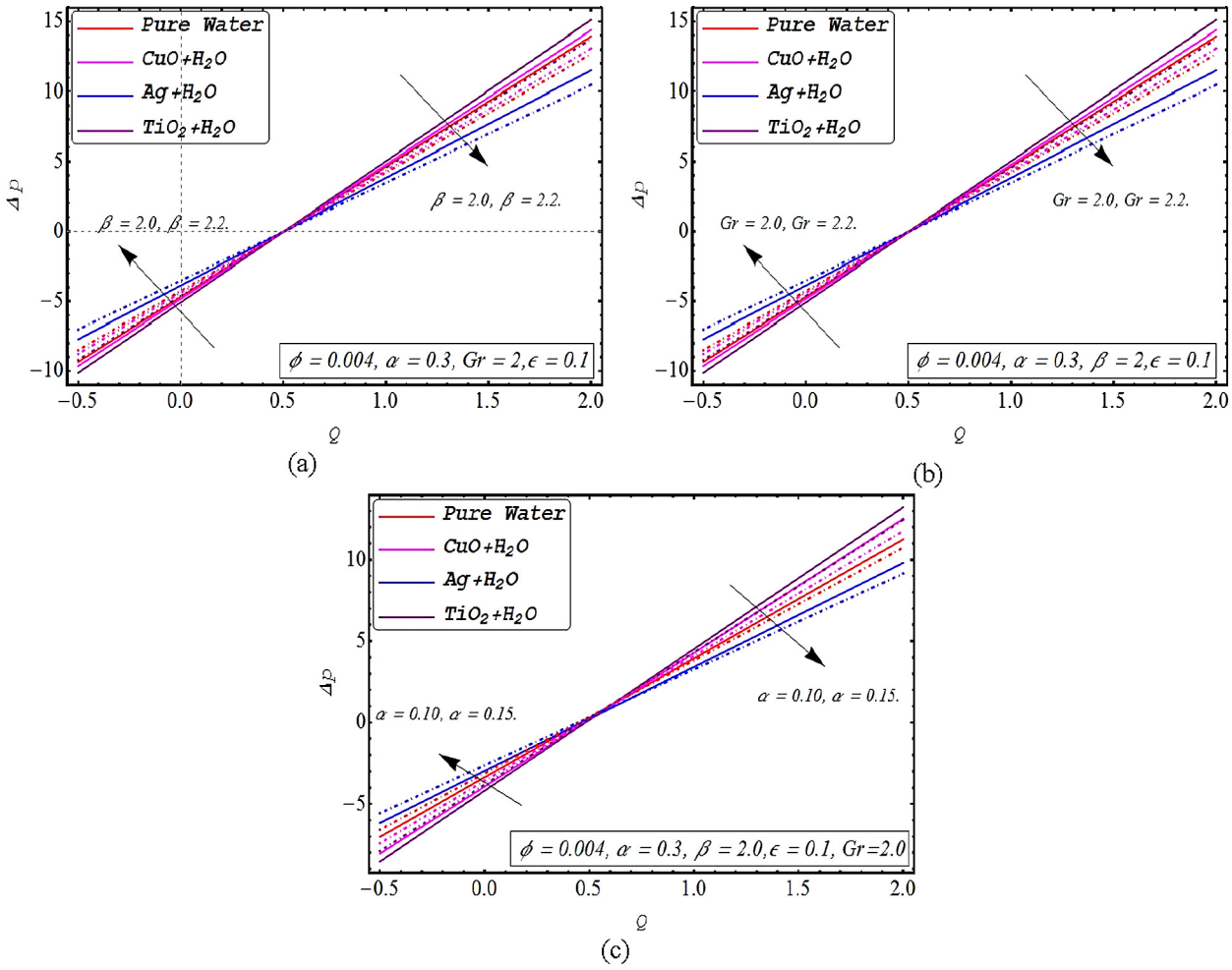


**Fig. 5.** Pressure rise $\Delta P$ against the flow rate $Q$ for different values of(a) $\beta = 2.0$ , 2.2. (b) $Gr = 2.0$, 2.2 and (c) $\alpha = 0.10$, 0.15. (Red line Pure water ——— Purple line Cuo + $H_2O$ ——— Blue line Ag + $H_2O$ ——— Dark Purple line TiO2 + $H_2O$ ———). (For interpretation of the references to color in this figure legend, the reader is referred to the web version of this article.)

nano-particle suspension cases are considered. Pressure rise generally increases with an increase in heat absorption parameter ($\beta$), Grashof number ($G_r$) and also viscosity parameter $\alpha$ in the *peristaltic pumping region* which corresponds to the volumetric flow rate range, $-0.5 \leqslant Q \leqslant 0.5$. However in *the augmented pumping region*, which approximately corresponds to the range, $0.5 < Q \leqslant 2$. in which is $0.51 \leqslant Q \leqslant 2$ pressure rise decreases with an increase in Grashof number ($G_r$), heat absorption parameter ($\beta$), and viscosity parameter ($\alpha$), which is the reverse of the response in the peristaltic pumping region. In all the plots, the pressure rise-volumetric flow rate ($\Delta p - Q$) demonstrates a linear relationship. Minimum values are computed always at the lowest volumetric flow rate and are negative; maximum values arise at the maximum volumetric flow rate and are positive. In the peristaltic pumping region, Titanium oxide nanofluid consistently attains the minimal values of pressure rise, whereas in the augmented pumping region, it achieves the maximum pressure rise values. Conversely silver water nanofluid attains the maximum pressure rise in the peristaltic pumping region, whereas it achieves the minimum magnitudes in the augmented pumping region. The implication is that no single nanofluid achieves a maximum pressure rise in both pumping regions. Therefore designers may judiciously select different nanofluids to optimize pressure rise in different regions of the peristaltic flow.

Fig. 6(a)–(c) depicts the axial response in wall tube shear stress ($S_{rz}$) for pure water and three different nanofluids, for variation with different thermo-physical parameters. The oscillatory nature of peristaltic propulsion is clearly captured in the profiles, owing to the sinousoidal wave propagation along the flexible tube wall. It is evident that silver water nanofluid invariably achieves the highest shear stress magnitudes as compared with pure water and other nanofluids (copper oxide water, Titanium oxide water). This is consistent with the acceleration computed earlier in connection with Silver water nanofluid. The lowest shear stress is observed for the pure water case. Therefore it is established again that the presence of nano-particles serves to increase velocity and there by increase in shear stresses at the wall. Close inspection of the profiles reveals that in the first region, magnitudes of shear stress start decreasing at the entry point of the tube until a maximum constriction is reached and thereafter the shear stress magnitudes increase to the end of the contracting section in the range ($0 \leqslant z \leqslant 1$). This characteristic is also exhibited for subsequent regions i.e. ($1 \leqslant z \leqslant 2$ and $2 \leqslant z \leqslant 3$) i.e. it is repeated until the termination of the tube i.e. exit. Similar patterns are observed in all of Fig. 6(a)–(c). The figures respectively show that shear stresses are elevated with increasing heat source ($\beta$), Grashof number ($Gr$) and viscosity parameter ($\alpha$) i.e. the flow is accelerated at the inner wall of

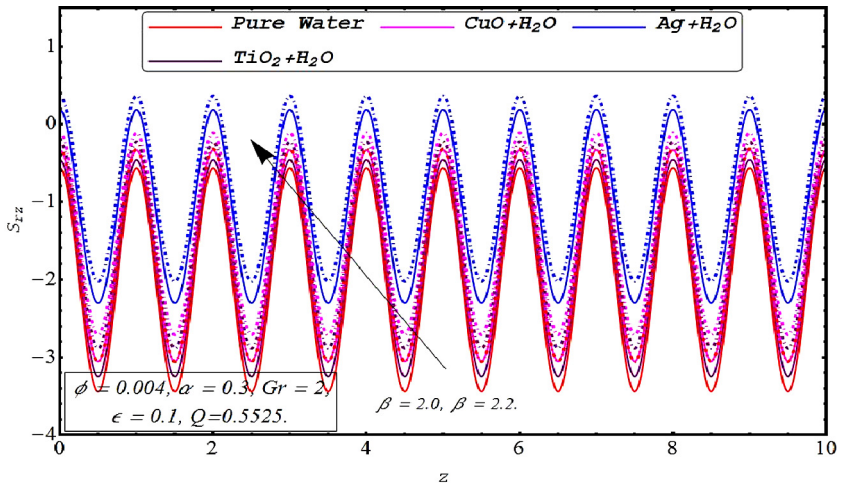


(a)

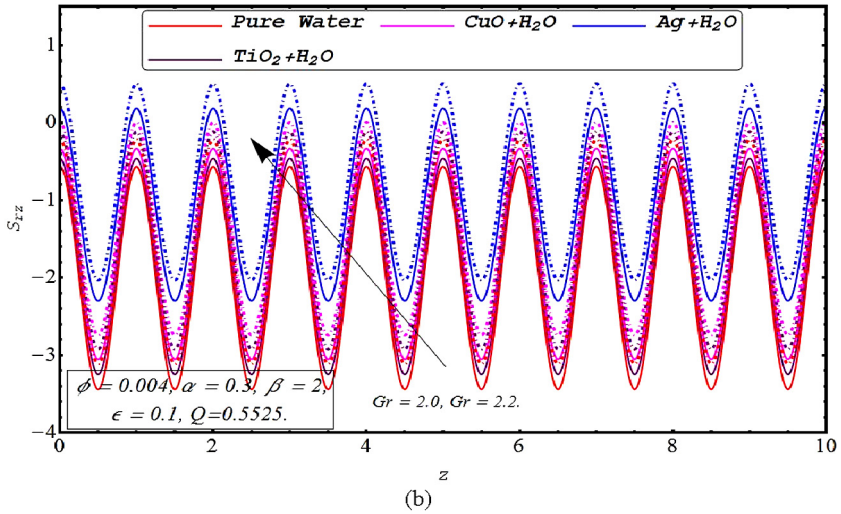


(b)

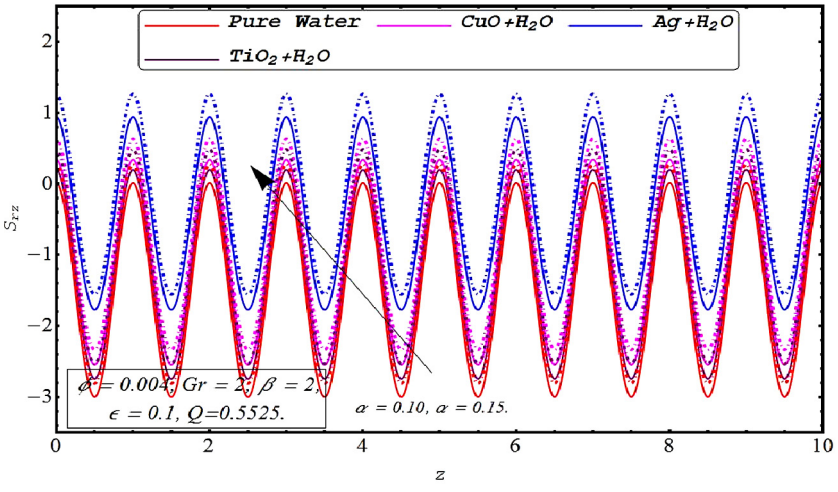


(c)

**Fig. 6.** Variation of wall shear stress $S_{rz}$ against axial distance $z$ for different values of (a) $\beta = 2.0$ , 2.2. (b) $Gr = 2.0$, 2.2 and (c) $\alpha = 0.10$, 0.15. (Red line Pure water ——— Purple line Cuo + $H_2O$ ——— Blue line Ag + $H_2O$ ——— Dark Purple line TiO2 + $H_2O$ ———). (For interpretation of the references to color in this figure legend, the reader is referred to the web version of this article.)

the tube with greater heat absorption, thermal buoyancy and decreasing viscosity of the nanofluid. These trends are indeed consistent with the earlier computations presented for axial velocity and also concur with other studies of nanofluid transport under peristaltic waves e.g. Akbar [14] and Nadeem, and Ijaz [36].

Figs. 7–14 depict streamline visualizations for the influence of different parameters in the peristaltic flow. These permit a better

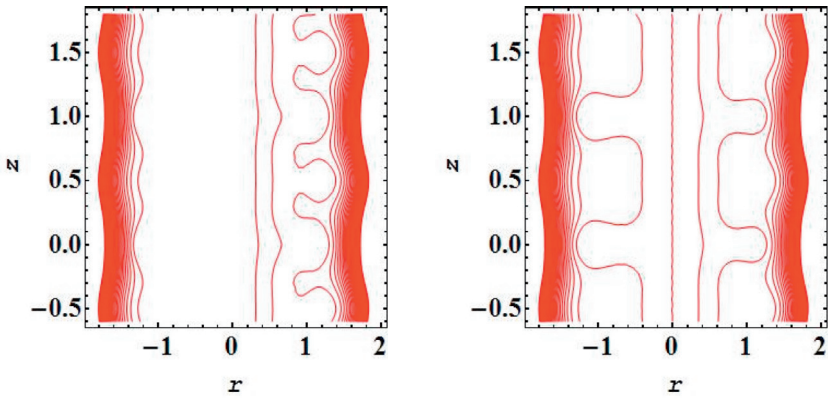


(a) $\beta = 2$ (b) $\beta = 2.2$

**Fig. 7.** Stream lines of Pure Water for different values of $\beta$

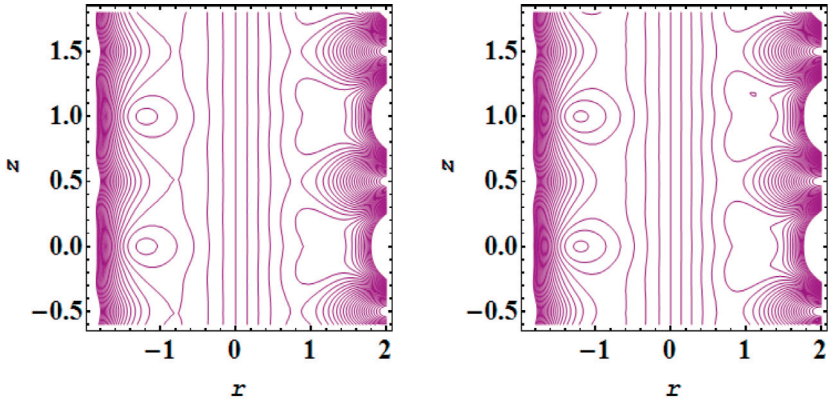


(a) $\beta = 2$ (b) $\beta = 2.2$

**Fig. 8.** Stream lines for CuO + $H_2O$ for different values of $\beta$

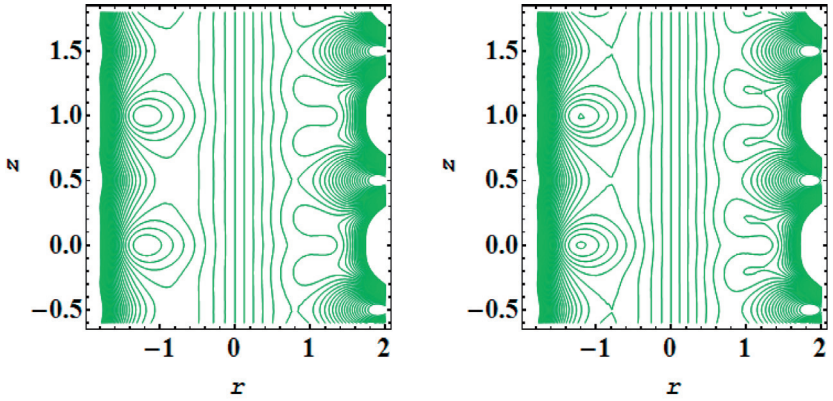


(a) $\beta = 2$ (b) $\beta = 2.2$

**Fig. 9.** Stream lines of $Ag$ + $H_2O$ for different values of $\beta$.

appraisal of the influence of trapping of boluses of nanofluid which is a characteristic phenomenon associated with creeping-type peristaltic dynamics. The effects of heat source parameter ($\beta$) on trapping phenomena for pure water $CuO + H_2O$ nanofluid and also $Ag$ + $H_2O$ nanofluid cases are presented respectively in Figs. 7a–9b. The number of trapped bolus increases with an increase in the value of heat source or sink parameter $\beta$ in all pure water, copper water and silver water nanofluids cases. Fig. 10(a)–(b) demonstrate that the quantity of trapped boluses decreases for the Titanium oxide water nanofluid ($Tio_2$ + $H_2O$) case with the increase of heat source parameter $\beta$.The modification in trapped phenomena again for pure water, CuO + $H_2O$ and $Ag$ + $H_2O$ nanofluids with variation in viscosity parameter ($\alpha$) are illustrated in Figs. 11a–13b respectively. The number of trapped boluses and also the size of the bolus *both increase* with an increase in viscosity parameter ($\alpha$) i.e. with *decreasing viscosity* of the nanofluid. Fig. 14a and b present the

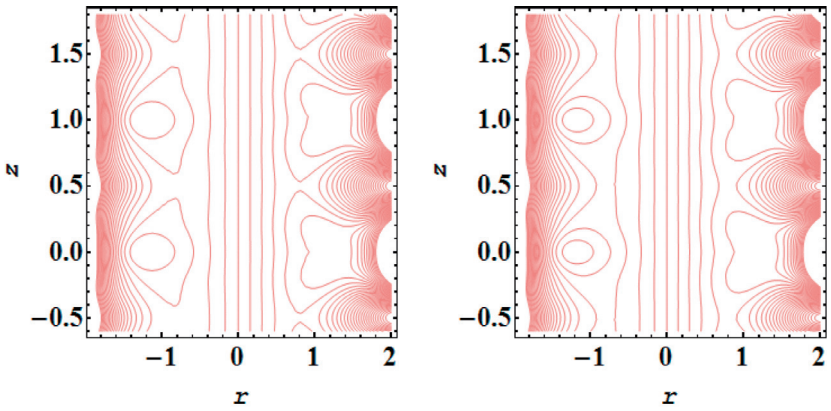


(a) $\beta = 2$ (b) $\beta = 2.2$

**Fig. 10.** Stream lines of $Tio_2 + H_2O$ for different values of $\beta$.

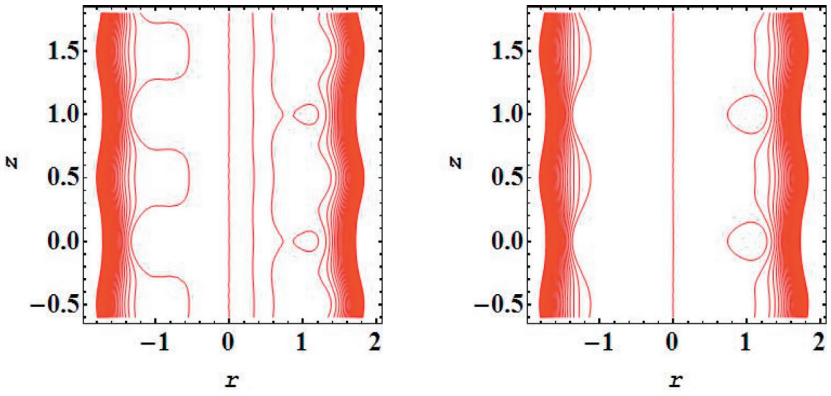


(a) $\alpha = 0.15$ (b) $\alpha = 2$

**Fig. 11.** Stream lines of Pure Water for different values of $\alpha$.

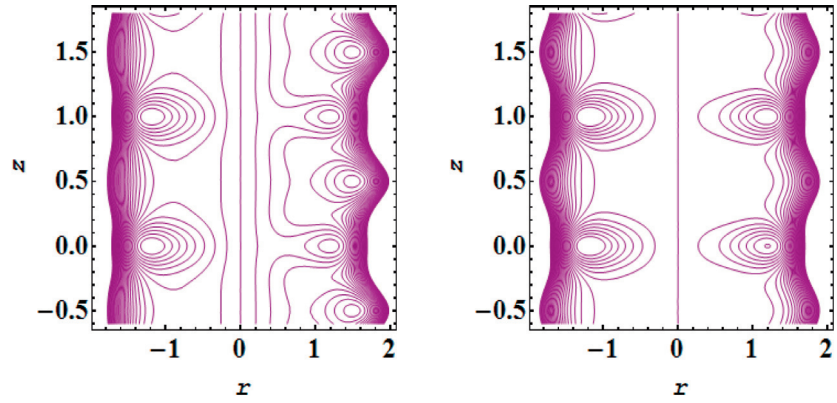


(a) $\alpha = 0.15$ (b) $\alpha = 2$

**Fig. 12.** Stream lines of $CuO + H_2O$ for different values of $\alpha$.

**Table 1**
Thermo-physical properties of pure water and other metallic nano-particles.

| Physical properties | $H_2O$ | CuO | Ag | $TiO_2$ |
|---|---|---|---|---|
| $c_p$ (J/kgK) | 4179.0 | 540.0 | 235 | 686.2 |
| $\rho$ (kg/m$^3$) | 997.1 | 6500.0 | 10500.0 | 4250.0 |
| $k$ (W/mk) | 0.613 | 18.0 | 429.0 | 401.0 |
| $\gamma \times 10^{-5}$(1/K) | 21.0 | 0.85 | 1.89 | 1.67 |

effects of viscosity parameter ($\alpha$) for $Tio_2 + H_2O$ nanofluid in the tube. The trapped bolus quantity decreases for the $Tio_2 + H_2O$ nanofluid case, with an increase in viscosity parameter $\alpha$ whereas the magnitude of the bolus markedly increases. Therefore different responses are observed for the different nano-particle cases. Tables 2–4 provide solutions for velocity and temperature functions, based on numerical evaluation of the closed-form solutions. They show that silver water nanofluid generally attains higher axial

**Table 2**
Variation of the velocity profile for different values of sink parameter P for pure water, CuO, Ag, and $TiO_2$ case.

| $w(r,z)$ | Pure water ($\phi = 0.00$) | | $CuO$ ($\phi = 0.004$) | | $Ag$ ($\phi = 0.004$) | | $TiO_2$ ($\phi = 0.004$) | |
|---|---|---|---|---|---|---|---|---|
| r | $\beta = 2$ | $\beta = 2.2$ | $\beta = 2$ | $\beta = 2.2$ | $\beta = 2$ | $\beta = 2.2$ | $\beta = 2$ | $\beta = 2.2$ |
| −0.9 | 0.0000 | 0.0000 | 0.0000 | 0.0000 | 0.0000 | 0.0000 | 0.0000 | 0.0000 |
| −0.7 | −0.1026 | −0.0928 | −0.0721 | −0.0629 | −0.0499 | −0.0382 | −0.0763 | −0.0677 |
| −0.5 | −0.2270 | −0.2146 | −0.1702 | −0.1585 | −0.1438 | −0.1288 | −0.1755 | −0.1644 |
| −0.3 | −0.3271 | −0.3142 | −0.2511 | −0.2389 | −0.2254 | −0.2098 | −0.2563 | −0.2448 |
| −0.1 | −0.3865 | −0.3736 | −0.2992 | −0.2871 | −0.2747 | −0.2591 | −0.3044 | −0.2928 |
| 0 | −0.4018 | −0.3889 | −0.3116 | −0.2995 | −0.2874 | −0.2718 | −0.3167 | −0.3052 |
| 0.2 | −0.3729 | −0.3599 | −0.2881 | −0.2759 | −0.2633 | −0.2477 | −0.2933 | −0.2817 |
| 0.4 | −0.3002 | −0.2873 | −0.2292 | −0.2171 | −0.2032 | −0.1876 | −0.2345 | −0.2231 |
| 0.6 | −0.1898 | −0.1778 | −0.1404 | −0.1292 | −0.1144 | −0.1001 | −0.1456 | −0.1349 |
| 0.8 | −0.0652 | −0.0574 | −0.0438 | −0.0365 | −0.0257 | −0.0163 | −0.0473 | −0.0404 |

**Table 3**
Variation of the velocity profile with different values of viscosity parameter ($\alpha$) for pure water, CuO, Ag and $TiO_2$ nanofluid cases.

| $w(r,z)$ | Pure water ($\phi = 0.00$) | | $CuO$ ($\phi = 0.004$) | | $Ag$ ($\phi = 0.004$) | | $TiO_2$ ($\phi = 0.004$) | |
|---|---|---|---|---|---|---|---|---|
| r | $a = 0.15$ | a = 2 | $a = 0.15$ | $a = 2$ | $a = 0.15$ | $a = 2$ | $a = 0.15$ | $a = 2$ |
| −0.9 | 0.0000 | 0.0000 | 0.0000 | 0.0000 | 0.0000 | 0.0000 | 0.0000 | 0.0000 |
| −0.7 | −0.1008 | 0.0089 | −0.0689 | 0.0698 | −0.0454 | 0.1833 | −0.0734 | 0.0504 |
| −0.5 | −0.2329 | −0.1569 | −0.1744 | −0.0588 | −0.1501 | 0.0631 | −0.1793 | −0.0794 |
| −0.3 | −0.3414 | −0.3321 | −0.2638 | −0.2104 | −0.2439 | −0.1076 | −0.2681 | −0.2273 |
| −0.1 | −0.4065 | −0.4462 | −0.3176 | −0.3115 | −0.3013 | −0.2249 | −0.3213 | −0.3254 |
| 0 | −0.4233 | −0.4766 | −0.3316 | −0.3385 | −0.3162 | −0.2564 | −0.3351 | −0.3516 |
| 0.2 | −0.3915 | −0.4193 | −0.3052 | −0.2876 | −0.2881 | −0.1971 | −0.3091 | −0.3022 |
| 0.4 | −0.3121 | −0.2824 | −0.2395 | −0.1669 | −0.2182 | −0.0577 | −0.2439 | −0.1851 |
| 0.6 | −0.1929 | −0.0994 | −0.1419 | −0.0111 | −0.1167 | 0.1135 | −0.1469 | −0.0322 |
| 0.8 | −0.0624 | 0.0362 | −0.0399 | 0.0816 | −0.0201 | 0.1767 | −0.0437 | 0.0653 |

**Table 4**
Variation of the Velocity profile for different values of nanoparticle volume fraction 0 for CuO, Ag, and $TiO_2$ case.

| $w(r,z)$ | $CuO$ | | $Ag$ | | $TiO_2$ | |
|---|---|---|---|---|---|---|
| r | $\phi = 0.01$ | $\phi = 0.04.$ | $\phi = 0.01$ | $\phi = 0.04$ | $\phi = 0.01$ | $\phi = 0.04$ |
| −0.9 | 0.0000 | 0.0000 | 0.0000 | 0.0000 | 0.0000 | 0.0000 |
| −0.7 | 0.1647 | 0.1419 | 0.1554 | 0.1168 | 0.1669 | 0.1486 |
| −0.5 | 0.2916 | 0.2511 | 0.2751 | 0.2067 | 0.2954 | 0.2631 |
| −0.3 | 0.3805 | 0.3277 | 0.3589 | 0.2698 | 0.3855 | 0.3433 |
| −0.1 | 0.4316 | 0.3716 | 0.4071 | 0.3059 | 0.4371 | 0.3894 |
| 0 | 0.4447 | 0.3829 | 0.4194 | 0.3152 | 0.4504 | 0.4012 |
| 0.2 | 0.4198 | 0.3616 | 0.3961 | 0.2976 | 0.4253 | 0.3788 |
| 0.4 | 0.3571 | 0.3075 | 0.3368 | 0.2531 | 0.3617 | 0.3222 |
| 0.6 | 0.2564 | 0.2208 | 0.2419 | 0.1818 | 0.2598 | 0.2314 |
| 0.8 | 0.1179 | 0.1015 | 0.1112 | 0.0835 | 0.1194 | 0.1063 |

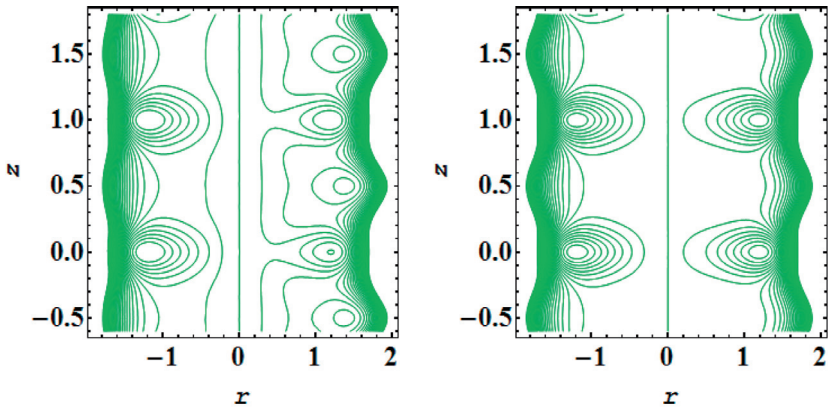

(a) $\alpha = 0.15$ (b) $\alpha = 2$

**Fig. 13.** Stream lines of $Ag + H_2O$ for different values of $\alpha$.

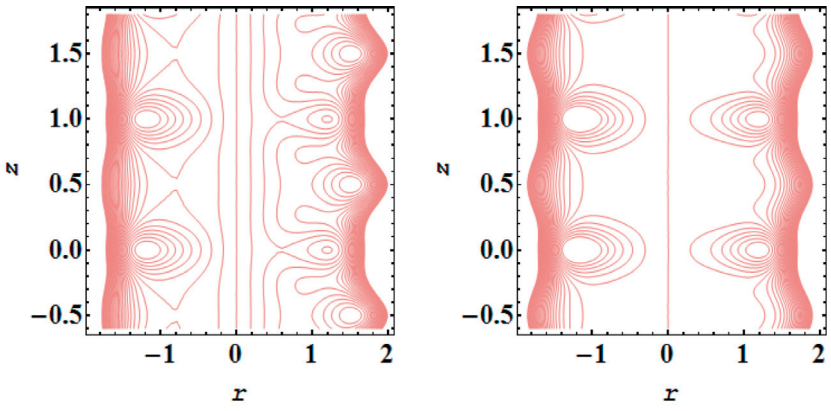


**Fig. 14.** Stream lines of $Tio_2 + H_2O$ for different values of $\alpha$.

velocities than the pure water or other nanofluid cases, provided the nano-particle volume fraction is the same i.e. $\phi = 0.004$. Maximum velocity and temperature, as shown and elaborated in earlier graphs, consistently arise at the centerline of the channel i.e. at $r = 0$. The temperature and velocity profiles always increase at the center of the tube with an increase in heat source parameter ($\beta$), viscosity parameter ($\alpha$) and also with the nanoparticle volume fraction ($\varphi$). Conversely the temperature and velocity magnitudes are found to fall in the near-wall regions of the tube.

## Conclusions

A mathematical study has been conducted of peristaltic propulsion and heat transfer in a temperature-dependent variable-viscosity nanofluid propagating through a flexible tube under thermal buoyancy and heat generation effect. The transformed boundary value problem has been linearized via appropriate creeping flow and long wavelength approximations and solved exactly. Numerical evaluation of the closed-form solutions has been conducted in symbolic software to evaluate the influence of heat source, Grashof number and viscosity parameter on axial velocity, axial pressure gradient, temperature, pressure rise, wall shear stress and also streamline plots. Pure water and also three nanofluid cases (Copper oxide-water, Silver-water and Titanium oxide water nanofluids) have been examined in detail. The computations have shown that.

(1) Increasing heat absorption parameter ($\beta$) generally accelerates the axial flow i.e. increases velocity and is greatest for silver-water ($Ag + H_2o$) nanofluid and lowest for pure water. The presence of nano-particles therefore aids the flow.
(2) Axial flow is decelerated with increasing Grashof number, ($G_r$) i.e. with greater thermal buoyancy force, with highest velocity magnitudes achieved by Silver-water nanofluid.
(3) Axial velocity is significantly increased with an increase in viscosity parameter ($\alpha$) i.e. with decreasing viscosity of the nanofluid, again with Silver water nanofluid achieving the highest acceleration.
(4) Temperature is elevated with heat absorption parameter ($\beta$) and is highest for pure water and lowest for Silver-water nanofluid.
(5) Temperature generally decreases significantly with increase in nanoparticle volume fraction ($\varphi$) i.e. nano-particles cool the regime and Silver water nanofluid demonstrates superior cooling to copper oxide nanofluid and Titanium oxide nanofluid.
(6) Axial pressure gradient is enhanced with *increasing viscosity parameter* ($\alpha$) i.e. decreasing viscosity. Maximum magnitudes are associated with Titanium oxide nanofluid whereas the lowest values are computed for Silver water nanofluid. Pressure gradient is lower for pure water as compared to Titanium oxide and Copper water nanofluids but higher than Silver water nanofluid.
(7) Axial pressure gradient decreases with greater heat absorption parameter ($\beta$) with highest values achieved by Titanium oxide and lowest values corresponding to Silver water nanofluid.
(8) Axial pressure gradient decreases substantially with increasing Grashof number, $G_r$ , throughout the length of the tube.
(9) Pressure rise *increases* with an increase in heat absorption parameter ($\beta$), Grashof number ($G_r$) and also viscosity parameter ($\alpha$) in the *peristaltic pumping region* i.e. the range $-0.5 \leqslant Q \leqslant 0.5$. However the opposite trend is observed in the *augmented pumping region* i.e. in the range $0.5 < Q \leqslant 2$, where pressure rise *decreases* with an increase in Grashof number ($G_r$), heat absorption parameter ($\beta$) and viscosity parameter ($\alpha$)
(10) Wall shear stress is a maximum for Silver water nanofluid and is minimized for the pure water case.
(11) The quantity of trapped boluses is elevated with an increase in the value of heat source parameter ($\beta$) for $CuO + H_2O$ nanofluid and also$Ag + H_2O$ nanofluid cases whereas it decreases for the Titanium oxide water nanofluid ($Tio_2 + H_2O$) case.
(12) The number of trapped boluses and also the size of the bolus *both increase* with an increase in viscosity parameter ($\alpha$) i.e. with *decreasing viscosity* of the nanofluid, for $CuO + H_2O$ and $Ag + H_2O$ nanofluids whereas the quantity of trapped boluses is reduced whereas the magnitude of the bolus markedly increases, for the $Tio_2 + H_2O$ nanofluid case, with an increase in viscosity parameter ($\alpha$).

The present study has overall provided a reasonable assessment of nano-particle influence on peristaltic nanofluid dynamics. It has however ignored *inclination* of the tube [39] and also *species diffusion* [40] which may be simulated via the Buonjiornio model [38]. These aspects will be considered in future investigations.

## References

[1] Fung YC. Biomechanics. New York, USA: Springer; 1990.
[2] Thain R. Movement of sugars through plants by cytoplasmic pumping. Nature 1969;222:873–5.
[3] Thompson MV. Scaling phloem transport: elasticity and pressure-concentration waves. J Theor Biol 2005;236:229–41.

[4] Ellahi R. Steady and unsteady flow for newtonian and non-newtonian fluids: basics, concepts and methods. Saarbrucken, Germany: VDM Press; 2009.
[5] Hameed M, Nadeem S. Unsteady MHD flow of a non-Newtonian fluid on a porous plate. J Math Anal Appl 2007;325:724–33.
[6] Tan WC, Masuoka T. Stokes' first problem for a second grade fluid in a porous half space with heated boundary. Int J Non-Linear Mech 2005;40:512–22.
[7] Tan WC, Masuoka T. Stokes first problem for an Oldroyd-B fluid in a porous half space. Phys Fluids 2005;17:023101–7.
[8] Tan WC, Masuoka T. Stability analysis of a Maxwell fluid in a porous medium heated from below. Phys Lett A 2007;360:454–60.
[9] Mahomed FM, Hayat T. Note on an exact solution for the pipe flow of a third grade fluid. Acta Mech 2007;190:233–6.
[10] Fetecau C, Fetecau C. On some axial Couette flows of non-Newtonian fluids. Z Angew Math Phys 2005;56:1098–106.
[11] Malik MY, Hussain A, Nadeem S. Flow of a Jeffrey-six constant fluid between coaxial cylinders with heat transfer. Commun Theor Phys 2011;56:345–51.
[12] Dehghan M, Shakeri M. The numerical solution of second Painlev'e equation. Numer Methods Partial Differ Equ 2009;25:1238–59.
[13] Nadeem S, Akbar NS. Effect of heat transfer on the peristaltic transport of MHD Newtonian fluid with variable viscosity: application of Adomian decomposition method. Commun Nonlinear Sci Numer Simul 2008;14:3844–55.
[14] Nadeem S, Akbar NS. Series solutions for the peristaltic flow of a Tangent hyperbolic fluid in a uniform inclined tube. Z Naturforsch 2010;65a:887–95.
[15] Dhumal R, Vidyapeeth B. Design and development of rotary peristaltic pump. Int J Sci Adv Tech 2012;2(4):8–15.
[16] Ejsing H. Peristaltic pumps- an answer to increasing demands within the biopharma industry. Eur Ind Pharm 2010;6:1–10.
[17] Diniz PHGD. Flow-batch analysis. TrAC, Trends Anal Chem 2012;35:39–49.
[18] Shukla JB, Gupta SP. Peristaltic transport of a power-law fluid with variable consistency. ASME J Biomech Eng 1982;104:182–6.
[19] Srivastava LM, Srivastava VP, Sinha SN. Peristaltic transport of a physiological fluid Part –I: Flow in Non-uniform geometry. Biorheology 1983;20:153–66.
[20] Hakeem AE, El Misiery AEM, Shamy IE. Effects of an endoscope and fluid with variable viscosity on peristaltic motion. Appl Math Comput 2004;158:497–511.
[21] Hakeem AE, El Misiery AEM, Shamy IE. Hydromagnetic flow of fluid with variable viscosity in uniform tube with peristalsis. J Phys A: Math Gen 2003;36:8535–47.
[22] Khan AA, Ellahi R, Usman M. The effects of variable viscosity on the peristaltic flow of non-Newtonian fluid through a porous medium in an inclined channel with slip boundary conditions. J Porous Media 2013;16:59–67.
[23] Akbar NS. Metallic nanoparticles analysis for the peristaltic flow in an asymmetric channel with MHD. IEEE Trans Nanotechnol 2014;13:357–61.
[24] Choi SUS. Enhancing thermal conductivity of fluids with nanoparticles, Developments and applications of non-Newtonian flows. In: Siginer DA, Wang HP, editors, 36. ASME; 1995. p. 99–105.
[25] Harris DL, Graffagnini MJ. Nanomaterials in medical devices: a snapshot of markets, technologies and companies. Nanotechnol Law Bus Winter 2007;415:422.
[26] Fullstone G, Wood J, Holcombe M, Battaglia G. Modelling the transport of nanoparticles under blood flow using an agent-based approach. Nat Sci Rep 2015;5(10649):1–13.
[27] Tan J, Thomas A, Liu Y. Influence of red blood cells on nanoparticle targeted delivery in microcirculation. Soft Matter 2012;8:1934–46.
[28] Tripathi D, Anwar Bég O. A study on peristaltic flow of nanofluids: Application in drug delivery systems. Int J Heat Mass Trans 2014;70:61–70.
[29] Ebaid A, Aly EH. Exact analytical solution of the peristaltic nanofluids flow in an asymmetric channel with flexible walls and slip condition: application to the cancer treatment. Comput Math Methods Med 2013;2013:825376.
[30] Akbar NS, Nadeem S, Hayat T, Hendi AA. Peristaltic flow of a nanofluid with slip effects. Meccanica 2012;47:1283–94.
[31] Akbar NS, Nadeem S. Peristaltic flow of a Phan-Thien-Tanner nanofluid in a diverging tube. Heat Transfer 2012;41:10–22.
[32] Anwar Bég O, Tripathi D. Mathematica simulation of peristaltic pumping with double-diffusive convection in nanofluids: a bio-nano-engineering model. Proc. IMECHE- Part N, J. Nanoeng Nanosyst 2012;225:99–114.
[33] Tiwari RK, Das MK. Heat transfer augmentation in a two-sided lid-driven differentially-heated square cavity utilizing nanofluids. Int J Heat Mass Transfer 2007;50:2002–18.
[34] Reynolds O. On the theory of lubrication and its application to Mr. Beauchamp Tower's experiments, including an experimental determination of the viscosity of olive oil. Phil Trans Royal Soc London 1886;177:157–234.
[35] Nadeem S, Ijaz S. Single wall carbon nanotube(SWCNT) examination on blood flow through a multiple stenosed artery with variable nanofluid viscosity. AIP Adv 2015;5:107217.
[36] Nadeem S, Ijaz S, Sadiq MA. Inspiration of induced magnetic field on a blood flow of Prandtl nanoáuid model with stenosis. Curr Nanosci 2014;13:753–65.
[37] Nadeem S, Ijaz S. Nanoparticles analysis on the blood flow through a tapered catheterized elastic artery with overlapping stenosis. Eur Phys J Plus 2014;129:249.
[38] Buongiorno J. Convective transport in nanofluids. ASME J Heat Transfer 2006;128(3):240–50.
[39] Tripathi D, Bég OA. MATHEMATICA numerical simulation of peristaltic biophysical transport of a fractional viscoelastic fluid through an inclined cylindrical tube. Comput Methods Biomech Biomed Eng 2015;18:1648–57.
[40] Anwar Bég O, Uddin MJ, Khan WA. Bioconvective non-Newtonian nanofluid transport in porous media containing micro-organisms in a moving free stream. J Mech Med Biol 2015;15:1550071.1–1550071.20.
[41] Nadeem S, Sadaf H, Adil Sadiq M. Analysis of nanoparticles on peristaltic flow of prandtl fluid model in an endoscopy. Curr Nano Sci 2015;11(6):709–21.
[42] Sadaf H, Nadeem S. Influences of slip and Cu-blood nanofluid in a physiological study of cilia. Comput Methods Programs Biomed 2016;131:169–80.
[43] Nadeem S, Sadaf H. Ciliary motion phenomenon of viscous nanofluid in a curved channel with wall properties. Eur Phys J Plus 2016;131:65.
[44] Nadeem S, Sadaf H. Hypothetical analysis for peristaltic transport of metallic nanoparticles in an inclined annulus with variable viscosity. Bull Polish Acad Sci Tech Sci 2016;64:447–54.